Title
Persistent Inter-Excitonic Quantum Coherence in CdSe Quantum Dots.

Journal
The journal of physical chemistry letters, 5(1)

ISSN
1948-7185

Authors
Caram, Justin R
Zheng, Haibin
Dahlberg, Peter D
et al.

Publication Date
2014

DOI
10.1021/jz402336t

Peer reviewed

THE JOURNAL OF PHYSICAL CHEMISTRY Letters

Letter

pubs.acs.org/JPCL

Persistent Interexcitonic Quantum Coherence in CdSe Quantum Dots

Justin R. Caram,[†] Haibin Zheng,[†] Peter D. Dahlberg,[‡] Brian S. Rolczynski,[†] Graham B. Griffin,[†] Andrew F. Fidler,[†] Dmitriy S. Dolzhnikov,[§] Dmitri V. Talapin,[§] and Gregory S. Engel*[,†]

[†]Department of Chemistry, The Institute for Biophysical Dynamics, and The James Franck Institute, [‡]Graduate Program in the Biophysical Sciences, The Institute for Biophysical Dynamics, and The James Franck Institute, and [§]Department of Chemistry, and The James Franck Institute, The University of Chicago, Chicago, Illinois 60637, United States

Supporting Information

ABSTRACT: The creation and manipulation of quantum superpositions is a fundamental goal for the development of materials with novel optoelectronic properties. In this Letter, we report persistent (~80 fs lifetime) quantum coherence between the 1S and 1P excitonic states in zinc-blende colloidal CdSe quantum dots at room temperature, measured using two-dimensional electronic spectroscopy. We demonstrate that this quantum coherence manifests as an intradot phenomenon, the frequency of which depends on the size of the dot excited within the ensemble of QDs. We model the lifetime of the coherence and demonstrate that correlated interexcitonic fluctuations preserve the relative phase between excitonic states. These observations suggest an avenue for engineering long-lived interexcitonic quantum coherence in colloidal quantum dots.

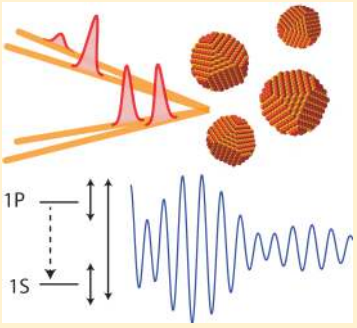

SECTION: Spectroscopy, Photochemistry, and Excited States

Zero-dimensional semiconductor nanocrystals, or quantum dots (QDs), have size-tunable quantum states that permit the development of useful optoelectronic properties.[1,2] QDs already contribute to imaging,[3−5] quantum information,[6,7] and electronic[8,9] technologies. Quantum confinement in these systems creates discrete, well-separated electron and hole states, shifting the band edge photoluminescence and establishing distinct absorption features corresponding to specific excitonic states.[10,11] These states can be individually optically addressed, resulting in different dynamic nonlinear responses to excitation.[12−14]

Recently, interexcitonic quantum coherence was reported between the two lowest-lying excitonic states in a room-temperature QD ensemble.[15] In these two excitonic states, the electron resides in its lowest excited state while the hole is in its lowest-energy or second-lowest-energy state. This coherence persisted with a dephasing time of 15 fs; the measurement was perhaps limited by ultrafast charge carrier relaxation due to the high density of states within the hole band or by inhomogeneous, ensemble sources of dephasing.[16,17] Interexcitonic quantum coherence has been implicated in enhancing energy transfer,[18−21] singlet fission,[22,23] multiple exciton generation,[24−26] and as a platform for quantum information.[7,9,27−31] Creation and optimization of quantum superpositions is desirable for technological applications and for understanding the fundamental optoelectronic properties of QDs.

In this Letter, we report direct signatures of quantum coherence between the band edge excitons and the first excited electron state, probed using continuum two-dimensional electronic spectroscopy (C-2DES). This coherence manifests as discrete, high-amplitude oscillations in two-dimensional spectra, which persist for ~80 fs. We use "persistent" to describe this coherence because it has a longer lifetime than the ground−excited state coherence as defined by the homogeneous line width. This relatively long lifetime permits a detailed analysis of this signal using its location on the 2D spectrum, its beat frequency, and its corresponding decay rate. By analyzing a 10% polydisperse sample, we identify coherent oscillations within an ensemble of quantum dots, with distinct size-dependent signatures. Analyzing these beat signatures, we ascertain if the coherence is excitonic or vibrational in nature and develop a simple model that describes the lifetime of the coherence. This model illustrates that intradot correlated fluctuations may maintain relative phase between excited states and suggests that dephasing is dominated by charge carrier relaxation. We estimate a cross-correlation coefficient of between 0.89 and 0.99 and discuss how intradot coherence among electronic excited states may be optimized.

A sample of oleic-acid-stabilized zinc-blende CdSe QDs (r = 3.0 ± 0.3 nm) was synthesized following the procedure of Chen et al.[32] and characterized using transmission electron microscopy and powder X-ray diffraction (see the Supporting Information and Figure S1a and S1b). We study zinc-blende QDs to limit the influence of disorder from excitonic fine structure brought about by crystal field splitting.[10] In Figure 1a, we show the first four excitonic states probed in this experiment, and in Figure 1b, we plot the absorption spectrum

Received: October 29, 2013
Accepted: December 9, 2013
Published: December 9, 2013

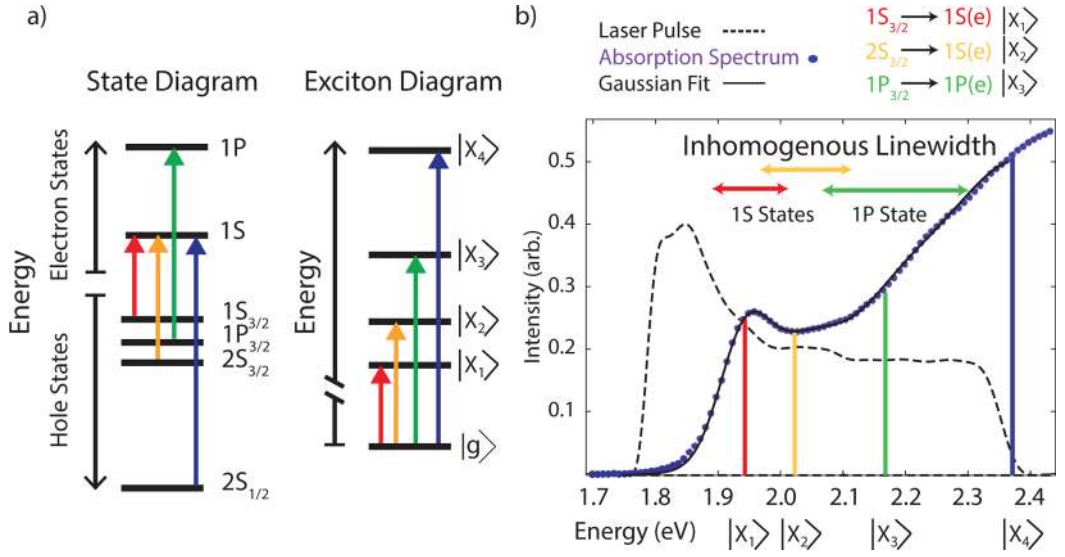

Figure 1. (a) QD states and their corresponding exciton transitions probed in this experiment. The first four hole states and first two electron states become the first four dipole-allowed transitions. (b) Absorption spectrum for zinc-blende CdSe quantum dots, fit to a five-Gaussian function, plotted alongside the laser pulse spectrum. We emphasize the three lowest-energy transitions, for which we plot the approximate inhomogeneous line widths given by eq 2. The 1S states ($|X_1\rangle$ and $|X_2\rangle$) show some overlap, with separation from the 1P ($|X_3\rangle$) state. The inhomogeneous line width is not centered over the transition due to the skewed Gaussian described by eq 1

of the sample. We fit this spectrum to a sum of five Gaussians (Figure S2, Supporting Information), representing the first five excitonic transitions, with energies consistent with previous assignments for dots of this size and comparable to more monodisperse dot preparations.[33−35] The spectrum of the laser pulse overlaps primarily with the first three excitonic features. During optical excitation, an electron is excited to the conduction band, leaving a corresponding hole in the valence band. These features are defined according to the hole (h) and electron (e) excited state that is populated and labeled $|X_1\rangle$ to $|X_4\rangle$ according to previous conventions, as shown in Figure 1a.[1,35−38] Many theoretical methods have been used to characterize QD excitonic states.[10,11,39,40] The simplest approximation, the effective mass model, describes each state with a principle quantum number (1, 2, 3, ...), an orbital angular quantum number (S, P, D, ...), and an overall angular moment (3/2, 1/2).[41] We label the lowest-lying band edge exciton $1S_{3/2}(h) \rightarrow 1S(e)$ as $|X_1\rangle$, followed by $2S_{3/2}(h) \rightarrow 1S(e)$ as $|X_2\rangle$, which differ only by the hole state excited. For simplicity, we collectively refer to these states by their electronic character, as 1S. The next transition, $1P_{3/2}(h) \rightarrow 1P(e)$, or $|X_3\rangle$, creates a new electron−hole pair in states that have different angular momentum, which we collectively refer to as 1P. The other 1P states are out of the laser bandwidth. The highest-energy excited state likely represents the split-off band, $2S_{1/2}(h) \rightarrow 1S(e)$, or $|X_4\rangle$, though we could not obtain reliable fits of the higher-energy states for this ensemble.

Both homogeneous and inhomogeneous broadening influence discrete features in QD absorption spectra. For example, QDs interact with phonons, ligands, and the solvent environment, which leads to pure dephasing of coherence as individual QDs undergo significant fluctuations and relaxation on the time scale of the measurement.[42−45] These same interactions also drive charge carrier relaxation, which homogenously broadens higher-energy features. Furthermore, near the band edge, charge carriers relax via different mechanisms, with holes displaying size-independent phonon-assisted relaxation, while electrons show size-dependent auger-like energy dissipation via electron−hole correlated motion.[12,39,46]

QDs also display significant static inhomogeneity arising from size and shape polydispersity and unresolved excitonic fine structure.[47] We can model size inhomogeneity using the particle in a spherical potential model, which neglects valence and conduction band mixing and overall angular momentum but captures the effect of polydispersity in particle line shapes.[10,41] If we know the central transition energy for a given state (from prior fitting), the distribution of energies for that state as a function of a Gaussian distribution of radii is given by

$$P(E) = \exp\left(-\frac{r_0^2(\sqrt{\Delta E_a/E} - 1)^2}{2\sigma^2}\right) \quad (1)$$

where r_0 and σ are the mean and the standard deviation of the particle radius distribution, respectively, and ΔE_a is the difference between the exciton energy and the bulk material band gap. Equation 1 results in a skewed Gaussian inhomogeneous line shape for a Gaussian distribution of particles. We express the full width at half-maximum (fwhm) of each state in eq 2, similar to an expression derived by others[48]

$$\text{fwhm} = 2\sqrt{2\log 2}\,\frac{2\Delta E_a r_0^3 \sigma}{(a_0^2 - 2\log(2)\sigma^2)^2} \quad (2)$$

Within this model, both the energy of a state above the band edge and the particle size distribution contribute to the ensemble line shape. Put simply, larger particles have more closely spaced excitonic states than smaller particles, which leads to concomitant effects on ensemble line shapes, with higher-energy states showing far broader inhomogeneous line widths than lower-energy states. This relationship has been confirmed experimentally in size-dependent studies of QD state energies.[35,36] We plot the estimated inhomogeneous line width from eq 3 for the first three states in our ensemble of QDs in Figure 1, above the absorption spectrum. The two band edge

dx.doi.org/10.1021/jz402336t | J. Phys. Chem. Lett. 2014, 5, 196−204

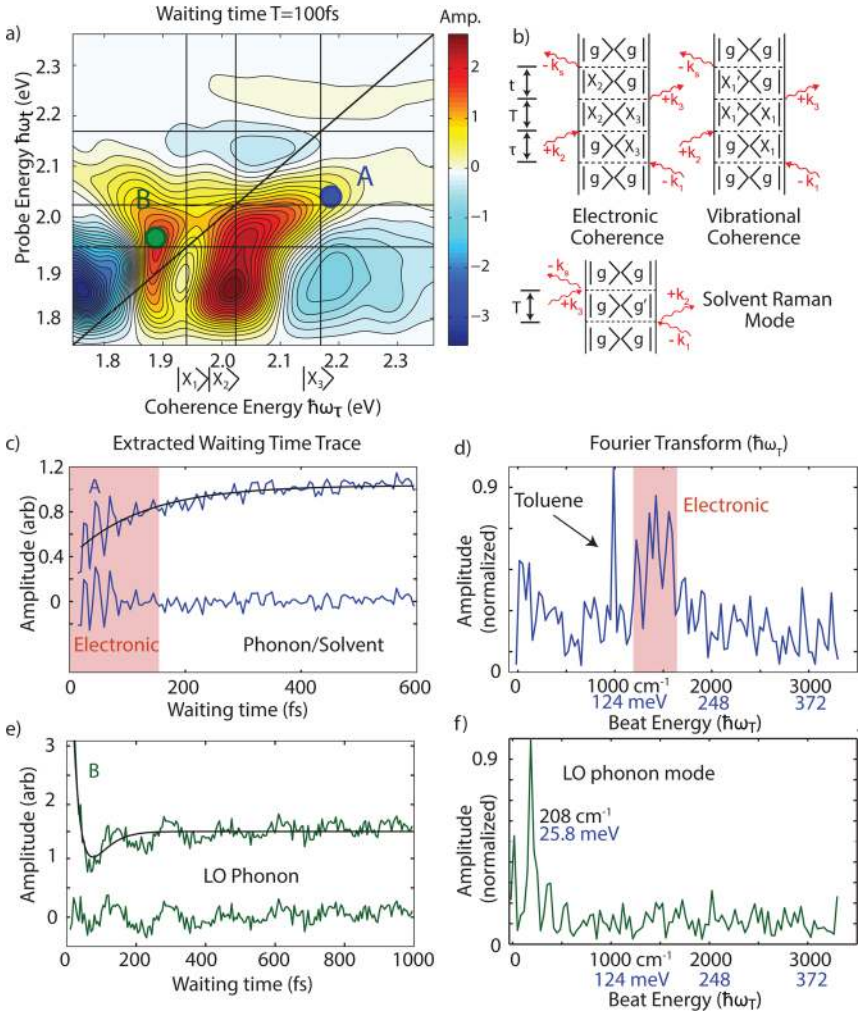

Figure 2. (a) Two-dimensional spectrum, with A representing the 1P/1S cross-peak and B highlighting the band edge feature. (b) Feynman diagrams representing stimulated emission coherent oscillatory (rephasing $\tau > 0$) contributions to the signal and coherent solvent response. The arrows represent electric field interactions, which interact with the density matrix of the ensemble. Coherences are off-diagonal elements of the density matrix, which during the waiting time create oscillatory signals in 2D spectra. (c) We plot the raw signal from A and the residual upon subtraction of a two-fit exponential representing population dynamics during the waiting time. This shows large-amplitude early time coherent response, followed by smaller-amplitude oscillatory signals. (d) A Fourier transform of the residual signal showing a broad peak centered at 1500 cm^{-1}, assigned in this work to electronic coherence, and a narrow peak near 1000 cm^{-1}, which we assign to the dominant Raman-active mode in toluene. We attribute the apparent structure underneath of the electronic coherence to additional solvent modes or to experimental noise. (e,f) The same analysis as that in (c) and (d) for the band edge feature B, which oscillates with the longitudinal optical phonon mode.

1S states show considerable overlap, while the third 1P state is well-resolved despite displaying twice the width of the band edge exciton. In accordance with the particle in a sphere model, large dots have smaller energy gaps between states than small dots. Excitonic coherences induce waiting time domain oscillations in 2D spectra, at a frequency difference equal to the energy gap between two states; thus, larger dots will result in slower oscillations compared to smaller dots.

In this work, we use 2DES to probe beneath the inhomogeneous line shape and to resolve particle-size-dependent signatures of excitonic coherence. 2DES has been extensively reviewed elsewhere and has recently been applied to study quantum dot dynamics.[15,49−52] In this Letter, we use a variant of 2DES, C-2DES, which utilizes ultrafast filament generation in argon to generate broad-band, stable "white" light (0.5% std/mean measured at 10 Hz) as an excitation and probe field. We describe the details of the C-2DES apparatus elsewhere and show a schematic of the apparatus in the Supporting Information (Figure S3).[53] We compress the spectral region from 520 to 700 nm to sub-10 fs pulses, using multiphoton intrapulse interference phase scan (MIIPS) with a spatial light modulator; the pulse duration is confirmed using transient grating frequency-resolved optical gating (Figure S4, Supporting Information).[54,55] Using beamsplitters, we then create three pulses. Time delays between pulses are systematically varied to generate 2D spectra.[56−59] The evolution of the system during the time, τ, between the first two pulses can be Fourier transformed to determine the energy of the input (the "coherence energy" domain). The system then evolves unperturbed as an excited- or ground-state population or as a coherence for a waiting time, T. The third pulse probes the system, driving subsequent emission in a phase-matched direction that is heterodyned with a local oscillator pulse and spectrally resolved (defining the "probe energy" axis). In a typical experiment, signal is collected for τ ranging from −60 to 80 fs, and 2D spectra are measured for T = 0−1000 fs in 5 fs

dx.doi.org/10.1021/jz402336t | J. Phys. Chem. Lett. 2014, 5, 196−204

Table 1. Parameters Derived from Fitting Equations 3 and 4 for Early Time Oscillations from the 1P/1S Cross-Peak

	amplitude	frequency	lifetime	correlation factor[a]
C	$a_1 = 1.0 \pm 0.27$[b]	$\omega_1 = 1440 \pm 25$ cm^{-1}	$T_1 = 70 \pm 23$ fs	$C_1 = 0.97$ (0.94–0.983)
	$a_2 = 1.1 \pm 0.30$[c]	$\omega_2 = 946 \pm 32$[c]	$T_2 = 55 \pm 17$[c]	null
D	$a_1 = 0.6 \pm 0.29$	$\omega_1 = 1704 \pm 36$	$T_1 = 85 \pm 50$	$C_1 = 0.97$ (0.89–0.99)
	$a_2 = -1.0 \pm 0.27$	$\omega_2 = 2019 \pm 20$	$T_2 = 97 \pm 36$	$C_2 = 0.98$ (0.96–0.99)

[a]The degree of correlation (C) is approximated by fitting eq 4 to reproduce the decay rate estimated by the fit as discussed in the text. The numbers in parentheses represent the correlation needed to reproduce the low and high range for the decay rate. [b]Errors reported are standard deviations for experimental fits. [c]We assign ω_2 from feature C to a nonresonant toluene solvent mode.

steps (data processing methodology discussed in the Supporting Information and shown in Figure S5). The dynamics during T reflect both relaxation of charge carriers (leading to exponential growth or a decrease in signals) and oscillatory dynamics, arising from phonon and electronic superposition states. Using combined rephasing ($\tau > 0$) and nonrephasing ($\tau < 0$) signals, we can assign features in 2D spectra to ground-state bleach, stimulated emission from the excited state, and induced excited-state absorption, which represents biexcitonic features, in analogy to transient absorption measurements.[15,60−62] To assign phase to these features, we fit the 2D spectrum to separately collected pump−probe spectra in accordance with the projection slice theorem.[58,63] In this work, we focus on coherent dynamics, which appear both in the real (absorptive) 2D spectrum as well as absolute magnitude spectra. All experiments were repeated several times with similar results. We show a replicate trace in Figure S6 of the Supporting Information.

By resolving the excitation frequency, 2DES excels at probing coherent signatures.[18,51,64−72] In Figure 2a, we show a typical broadband two-dimensional spectrum of CdSe quantum dots taken at $T = 100$ fs (additional spectra in Figure S7, Supporting Information). In this publication, we focus on the coherent dynamics of the 1P/1S cross-peak below the diagonal. This feature appears as the 1P state relaxes to the band edge.[12,46] Briefly, we observe the SE feature grow on a time scale of approximately 167 fs (when the center of the feature is probed), consistent with previous measurements of Auger-like 1P to 1S charge carrier relaxation for particles of this size.[12,46,73] The recovered time scale provides an estimate of the size-dependent Auger recombination rate that we will use in our model below. Below this feature, we observe a negative signal that we assign to excited-state absorption into biexciton states, red-shifted and enhanced by increased surface trapping of hot carriers during Auger-like relaxation, similar to signals reported in state-resolved TA measurements.[74,75] The line shape and its incoherent dynamics are the topics of a separate manuscript.[76]

Double-sided Feynman diagrams in Figure 2b show three sources of coherent dynamics in these QDs.[64,77] The first diagram describes an electronic coherence, in which oscillations arise from direct excitation of a coherent superposition of two excitonic states. These coherences result in oscillations in the amplitude of the 2D spectrum at the spectral coordinates corresponding to excitation into $|X_3\rangle$ and emission from $|X_2\rangle$ as the waiting time increases. The oscillation frequency corresponds to the energy difference between the two excitonic states. The second diagram describes vibrational coherences, where a coherent phonon mode modulates the energy gap between electronic states participating in optical excitation. Distinguishing between electronic and vibrational quantum coherences in QDs is much simpler than that in molecular or supramolecular systems. Unlike the ∼3N vibrational modes in a molecule, QDs have a sparser vibrational manifold. The longitudinal optical phonon mode modulates the energy gaps with a frequency of 209 cm^{-1} in CdSe, and the only other accessible modes are much lower frequency acoustic modes.[13,47,78] Finally, the nonresonant solvent signal modulates the overall signal via a vibrationally activated optical Kerr effect and also contributes to the 2D signal.[79,80]

We observe these three oscillatory signals in 2DES of quantum dots. In Figure 2c, we show an extracted waiting time trace from the real part of the 2DES spectrum over the 1P/1S stimulated emission cross-peak (feature A). The signal shows clear biphasic signatures, a large early time oscillatory response for the first 175 fs (∼25% of the total signal) followed by a persistent, lower-amplitude oscillation. We fit this trace to two exponentials to eliminate waiting time dynamics, then we Fourier transform (FT) the residual signal. Figure 2d shows that the high-amplitude early time signal corresponds to a frequency response around 1500 cm^{-1}, while the low-amplitude oscillations signals manifest in the FT as a narrow peak at 990 cm^{-1}, consistent with the strongest Raman-active mode in toluene.[81] Figure 2e and f show trace B from the band edge feature, illustrating modulation consistent with a longitudinal optical phonon mode at 26 meV but no clear high-frequency features. The differential signatures of longitudinal optical phonon modes are consistent with previous models that show that the 1P state has significantly weaker coupling to the longitudinal optical phonon mode than the 1S state.[13]

In Figure 3, we focus on the early time coherent dynamics of the 1P/1S cross-peak. In Figure 3a, we show a 2D spectrum from $T = 130$ fs, from which we examine two points across the inhomogeneous line shape of the 1P/1S stimulated emission feature, as shown. On the right, we plot the time domain oscillations for the first 175 fs. Similar to previous methods, we fit this oscillation to two exponential decay sinusoids according the following equation:[15,82,83]

$$S(T) = \sum_{n=1}^{2} a_n \exp\left(-\frac{T}{T_n}\right) \sin(\omega_n T + \phi_n) \tag{3}$$

We plot the results of this fit in Figure 3b, illustrating that the signal is well-modeled by eq 3. In Table 1, we show the frequencies and decay rates observed. In the insets of Figure 3b, we show a FT of the early time data with lines at the dominant fit frequencies to show how the fit conforms to the FT. The fit and the FT demonstrate that at point C, we observe lower frequency signals than at point D, with both showing decay rates on the order of 80 fs. We assign the lowest-frequency feature in trace C (ω_2) to the previously discussed toluene mode.

In Figure 3c, we present the Fourier transforms of early waiting time data extracted across the 1P/1S SE feature. The dominant frequency varies continuously between 1300 and

dx.doi.org/10.1021/jz402336t | J. Phys. Chem. Lett. 2014, 5, 196−204

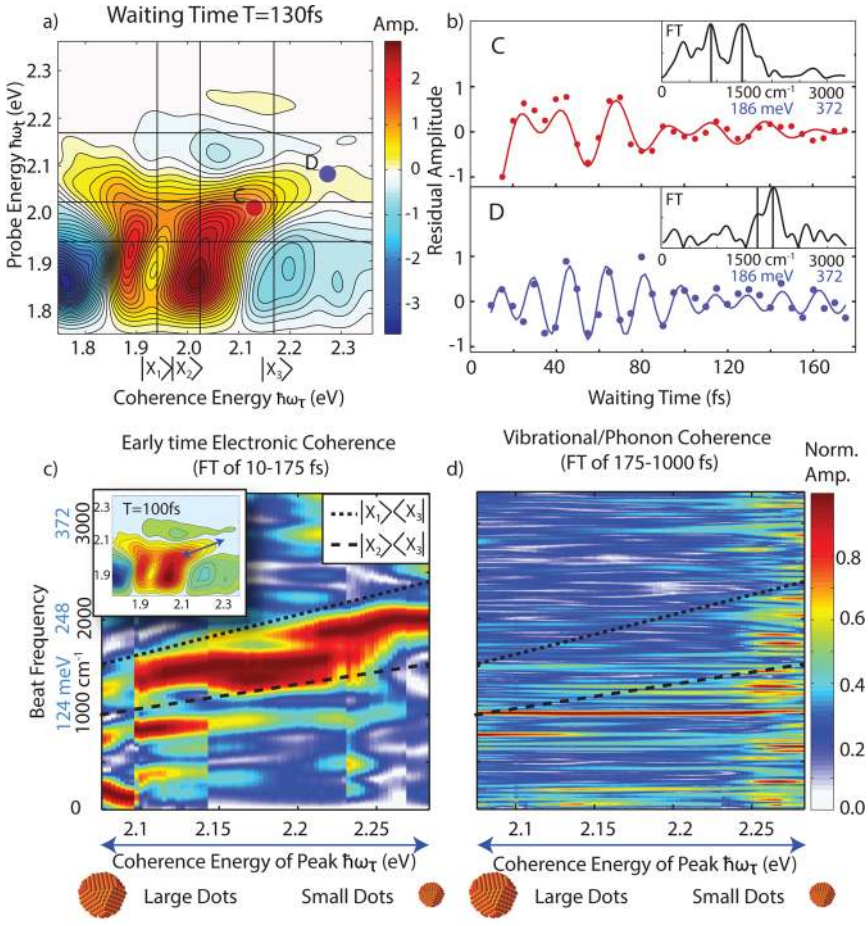

Figure 3. (a) 2D spectrum taken at T = 130 fs, highlighting two regions across the inhomogeneous bandwidth of the 1P/1S SE feature. (b) We plot the first 175 fs of the time domain of this feature (solid circles) after exponential subtraction. The solid lines represent the fit to eq 3. In the inset, we plot the Fourier transform of the early time signal, along with two lines representing the dominant fit frequencies. As can be observed, lower-frequency oscillations dominate at C versus higher frequencies at D. We show the parameters of each fit in Table 1. (c) We plot the Fourier spectrum of the residual early waiting time data for the entire inhomogeneous bandwidth of the 1P/1S stimulated emission cross-peak, normalized to each individual FT. Due to changes in phase in the oscillatory signal, vertical discontinuities arise from different exponential best-fit lines. The double-sided arrows in the inset show the region from which we extract the oscillatory signals. We observe a continuous increase in beating frequency ranging from 1300 to 2000 cm^{-1}. We overlay the expected energy differences between the 1P and 1S states $\langle |X_3\rangle/|X_2\rangle$ and $|X_3\rangle/|X_1\rangle\rangle$ across the range of particle sizes in our preparation of QDs (dashed lines). (d) We plot the same signal for the residual trace from 175 to 1000 fs, which shows little difference across the feature, illustrating coherent vibrational and phonon signatures.

2000 cm^{-1} and is proportional to the excitation energy as we progress along this feature. Lower input coherence energies display lower-frequency oscillations. We overlay the size-dependent expected energy difference between the 1P and both 1S excitonic states using the model presented in eq 2. Despite the ensemble measurement, we observe clear signatures of subensemble-resolved size-based heterogeneity in the coherent response, in particular, the slope of the oscillatory frequency across the feature. Put simply, the red edge of the cross-peak addresses larger dots, which have smaller difference energies, while the blue edge addresses smaller dots in the ensemble. Thus, the oscillatory signals can be identified as intradot electronic superpositions. Due to limited resolution in time, we cannot conclusively assign the coherence to a specific 1S state as both appear to contribute to the overall signal. We also plot the FT of the same feature from 175 to 1000 fs in Figure 3d, which shows no coherence-energy-dependent response, as expected for vibrational coherences.[72,84] Finally, in Figure S8 (Supporting Information), we show early time traces taken from the magnitude-only spectrum to show that the result does not arise from phasing error; we also plot the analogous upper diagonal feature for nonrephasing, rephasing, and combined pathways, showing signals consistent with electronic coherence using the method described by Turner et al.[15,72] Thus, the frequency, spectral character, position on the 2D spectrum, and time domain response allow us to assign the early time oscillation to the presence of a superposition between 1S and 1P excitonic states inside of an individual quantum dot.

The lifetime of a coherence measures the persistence of the relative phase between these states, informing on perturbations to that phase by fluctuations of the constituent energy levels and electronic relaxation.[85−89] It is not surprising that excitonic states fluctuate relative to one another in a manner quite distinct from the ground state.[90] This effect has been observed in photosynthetic systems, small molecules, and polymers.[18,91−94] We can understand the coherence lifetime (measured to be ∼80 fs) between two states, 1S and 1P, using a simple model (shown in Figure 4a) that considers fluctuations and relaxation as follows[95]

dx.doi.org/10.1021/jz402336t | J. Phys. Chem. Lett. 2014, 5, 196−204

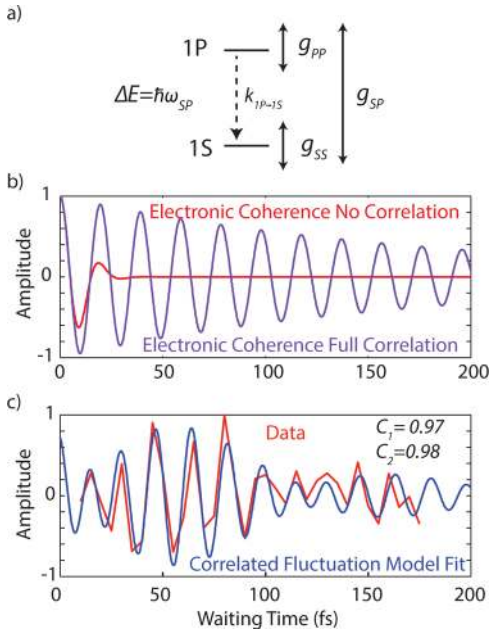

Figure 4. (a) A representation of the terms from eq 4; ω_{SP} represents the energy difference between states, $k_{1P\rightarrow1S}$ is the rate of relaxation, g_{SS} and g_{PP} are the line shape functions that represent the fluctuations of each state, and g_{SP} describes degree to which those fluctuations are shared (or correlated). (b) Two extreme cases, where the fluctuations are completely uncorrelated (leading to dephasing on a 10 fs time scale) or completely correlated (leading to dephasing only from population relaxation). (c) Data from point D from Figure 3, which shows two frequencies for which we fit the model described in Supporting Information, given known line shape parameters. The fit shows that a high degree of correlation (C = 0.97 or 0.98 for the two observed modes, respectively) is needed to reproduce the observed excitonic lifetimes.

$$\rho_{SP}(T) \propto \langle \exp[i\omega_{SP}T - g_{SS}(T) - g_{PP}(T) + 2\mathrm{Re}(g_{SP}(T)) - (k_{1P\rightarrow1S} + k_r + k_{nr})T]\rangle \quad (4)$$

Here, the evolution of the off-diagonal element of the density matrix $\rho_{SP}(T)$ is defined by an oscillatory component (ω_{SP}) that modulates the signal at the energy difference between 1S and 1P and several processes that dephase this coherence. We describe fluctuations via the line shape function for each individual state (g_{SS} and g_{PP}), which dephase the coherence.[96,97] Population relaxation from state P to state S also eliminates coherence and is represented by a rate $k_{1P\rightarrow1S}$. The radiative and nonradiative (k_r and k_{nr}) rates that govern 1S relaxation to the ground state are much slower (10−100 ns time scale) than the population relaxation rate and can be ignored.[98] The correlation between excitons, described by g_{SP}, increases the coherent lifetime due to coupling between the exciton states and a shared vibrational bath.[99]

To develop a simple model to estimate the expected lifetime in QDs, we make a few approximations and apply them to eq 4. First, we assume that $g_{SS} = g_{PP}$ and use previously measured photon echo peak shift measurements[44,100] to estimate the homogeneous line width. We then model the shared correlation as $C{\cdot}2{\cdot}g_{SS}$, where C represents the correlation of fluctuations in both states due to coupling between the excitons and a shared bath. The expected signal within this model is given by

$$S(T) = A_n \exp[i\omega_n T - 2(1 - C){\cdot}g_{SS}(T) - (k_{1P\rightarrow1S})T + \phi_n] \quad (5)$$

where A_n, ω_n, C, and ϕ_n are fitting parameters related to the amplitude, frequency, correlation, and phase, respectively. We estimate g_{SS} using the photon echo peak shift parameters reported by Salvador et al.[44] for the largest dots measured. While these dots are not identical to those used in this experiment, they assist in providing an estimate of the overall correlation. The parameters report on a spectral density from which the line shape can be estimated using standard methods.[77] Using the recovered relaxation time from above of $1/k_{1P\rightarrow1S}$ = 167 fs,[46,73] we fit C and show the estimates for the range of lifetimes defined in Table 1. This method allows for an examination of how C varies within the error of the liftime estimated by eq 3. Our calculation shows that near-unity correlation is required to explain the measured coherence lifetimes. If we assume no correlation between sites, the homogeneous line width dominates, leading to dephasing with a lifetime of approximately 10 fs. In a fully correlated bath, the coherence only dephases due to population relaxation with a lifetime of 167 fs. We plot these extremes and the fitted correlation in Figure 4b and c. We believe that due to wave function overlap, shared fluctuations are likely an intrinsic feature in colloidal QDs, significantly increasing the lifetime of excitonic coherences. This same mechanism has been implicated in anomalously long lifetimes in photosynthetic complexes,[85,88] though several other explanations for long-lived coherence have emerged.[101−104] This study demonstrates that despite homogeneous line widths of approximately 0.1 eV,[42,44] correlated fluctuations can significantly enhance the lifetime of quantum coherence in QDs.

Currently, charge carrier relaxation dominates the dephasing process for quantum dots. However, because 1S/1P coherence involves different electronic states, it may be possible to create far longer room-temperature QC using core−shell materials. For example, Pandey and co-workers have shown that electron cooling can be significantly slowed by putting a ZnSe shell on a CdSe dot, which decreases electron−hole wave function overlap, slowing Auger-like charge relaxation.[105] One can also tune the homogeneous line width via surface capping and passivation, with such dots showing significantly decreased homogeneous line widths.[45,100] Furthermore, the lifetime reported here represents merely a lower bound for the coherence lifetime because other forms of polydispersity (shape, ligand field, etc.) will lead to ensemble-dephasing of the signal, not distinguishable in our measurement.[17,106] Analysis of more monodisperse preparations, films, and probing the temperature dependence represents avenues for future research.

In summary, we demonstrate the presence of discrete oscillatory signals representing excitonic superpositions in quantum dots between the 1S and 1P states. These signals can be distinguished from other oscillatory signals (such as the longitudinal optical phonon mode) via their early time response, in agreement with interexciton size-dependent frequencies and their spectral position upon excitation of 1P and subsequently 1S states. The ability to resolve size-dependent inhomogeneity in a polydisperse solution illustrates the utility of C-2DES in resolving in-ensemble heterogeneity. We conclude that the persistent quantum coherence observed requires significant correlation in the fluctuations of each excitonic state.

dx.doi.org/10.1021/jz402336t | J. Phys. Chem. Lett. 2014, 5, 196−204

■ ASSOCIATED CONTENT

Supporting Information

We provide further information about instrumentation, data analysis, sample preparation, and modeling. This material is available free of charge via the Internet at http://pubs.acs.org.

■ AUTHOR INFORMATION

Corresponding Author

*E-mail: gsengel@uchicago.edu.

Notes

The authors declare no competing financial interest.

■ ACKNOWLEDGMENTS

The authors would like to thank NSF MRSEC (Grant No. DMR 08-02054), The Keck Foundation, Packard Foundation, DOE Sunshot (DE-EE005312), AFOSR (Grant No. FA9550-09-1-0117), and DTRA (HDTRA1-10-1-0091) for supporting this work. J.R.C. and P.D.D. acknowledge support from the NSF GRFP. A.F.F. acknowledges support from the DOE SCGF. P.D.D. was supported in part by the Graduate Program in Biophysical Sciences at the University of Chicago (National Institutes of Health Grant T32 EB009412).

■ REFERENCES

(1) Klimov, V. I. *Nanocrystal Quantum Dots*; CRC Press: New York, 2010.

(2) Alivisatos, A. P. Semiconductor Clusters, Nanocrystals, and Quantum Dots. *Science* **1996**, *271*, 933−937.

(3) Michalet, X.; Pinaud, F. F.; Bentolila, L. A.; Tsay, J. M.; S Doose, J. J. L.; Sundaresan, G.; Wu, A. M.; Gambhir, S. S.; Weiss, S. Quantum Dots for Live Cells, In Vivo Imaging, and Diagnostics. *Science* **2005**, *307*, 538−544.

(4) Gao, X.; Cui, Y.; Levenson, R. M.; Chung, L. W. K.; Nie, S. In Vivo Cancer Targeting and Imaging with Semiconductor Quantum Dots. *Nat. Biotechnol.* **2004**, *22*, 969−976.

(5) Bruchez, M.; Moronne, M.; Gin, P.; Weiss, S.; Alivisatos, A. P. Semiconductor Nanocrystals as Fluorescent Biological Labels. *Science* **1998**, *281*, 2013−2016.

(6) Gupta, J. A.; Knobel, R.; Samarth, N.; Awschalom, D. D. Ultrafast Manipulation of Electron Spin Coherence. *Science* **2001**, *292*, 2458−2461.

(7) Imamoglu, A.; Awschalom, D. D.; Burkard, G.; DiVincenzo, D. P.; Loss, D.; Sherwin, M.; Small, A. Quantum Information Processing Using Quantum Dot Spins and Cavity QED. *Phys. Rev. Lett.* **1999**, *83*, 4204−4207.

(8) O'Regan, B.; Gratzel, M. A Low-Cost, High-Efficiency Solar Cell Based on Dye-Sensitized Colloidal TiO_2 Films. *Nature* **1991**, *353*, 737−740.

(9) Coe-Sullivan, S. Optoelectronics: Quantum Dot Developments. *Nat. Photonics.* **2009**, *3*, 315−316.

(10) Efros, A. L.; Rosen, M. The Electronic Structure of Semiconductore Nanocrystals. *Annu. Rev. Mater. Sci.* **2000**, *30*, 475−521.

(11) Éfros, A. L. Density of states and interband absorption of light in strongly doped semiconductors. *Sov. Phys. Usp.* **1974**, *16*, 789.

(12) Kambhampati, P. Hot Exciton Relaxation Dynamics in Semiconductor Quantum Dots: Radiationless Transitions on the Nanoscale. *J. Phys. Chem. C* **2011**, *115*, 22089−22109.

(13) Sagar, D. M.; Cooney, R. R.; Sewall, S. L.; Dias, E. A.; Barsan, M. M.; Butler, I. S.; Kambhampati, P. Size Dependent, State-Resolved Studies of Exciton−Phonon Couplings in Strongly Confined Semiconductor Quantum Dots. *Phys. Rev.* **2008**, *77*, 235321.

(14) Sewall, S. L.; Cooney, R. R.; Dias, E. A.; Tyagi, P.; Kambhampati, P. State-Resolved Observation in Real Time of the Structural Dynamics of Multiexcitons in Semiconductor Nanocrystals. *Phys. Rev. B* **2011**, *84*, 235304.

(15) Turner, D. B.; Hassan, Y.; Scholes, G. D. Exciton Superposition States in CdSe Nanocrystals Measured Using Broadband Two-Dimensional Electronic Spectroscopy. *Nano Lett.* **2011**, *12*, 880−886.

(16) Griffin, G. B.; Ithurria, S.; Dolzhnikov, D. S.; Linkin, A.; Talapin, D. V.; Engel, G. S. Two-Dimensional Electronic Spectroscopy of CdSe Nanoparticles at Very Low Pulse Power. *J. Chem. Phys.* **2013**, *138*, 014705.

(17) Fidler, A. F.; Harel, E.; Long, P. D.; Engel, G. S. Two-Dimensional Spectroscopy Can Distinguish between Decoherence and Dephasing of Zero-Quantum Coherences. *J. Phys. Chem. A* **2011**, *116*, 282−289.

(18) Engel, G. S.; Calhoun, T. R.; Read, E. L.; Ahn, T.-K.; Mancal, T.; Cheng, Y.-C.; Blankenship, R. E.; Fleming, G. R. Evidence for Wavelike Energy Transfer through Quantum Coherence in Photosynthetic Systems. *Nature* **2007**, *446*, 782−786.

(19) Rebentrost, P.; Mohseni, M.; Kassal, I.; Lloyd, S.; Aspuru-Guzik, A. Environment-Assisted Quantum Transport. *New J. Phys.* **2009**, *11*, 033003.

(20) Abramavicius, D.; Mukamel, S. Quantum Oscillatory Exciton Migration in Photosynthetic Reaction Centers. *J. Chem. Phys.* **2010**, *133*, 064510.

(21) Caruso, F.; Chin, A. W.; Datta, A.; Huelga, S. F.; Plenio, M. B. Entanglement and Entangling Power of the Dynamics in Light-Harvesting Complexes. *Phys. Rev. A: At., Mol. Opt. Phys.* **2010**, *81*, 062346.

(22) Chan, W.-L.; Ligges, M.; Zhu, X. Y. The Energy Barrier in Singlet Fission Can Be Overcome through Coherent Coupling and Entropic Gain. *Nat. Chem.* **2012**, *4*, 840−845.

(23) Smith, M. B.; Michl, J. Singlet Fission. *Chem. Rev.* **2010**, *110*, 6891−6936.

(24) Beard, M. C.; Midgett, A. G.; Hanna, M. C.; Luther, J. M.; Hughes, B. K.; Nozik, A. J. Comparing Multiple Exciton Generation in Quantum Dots to Impact Ionization in Bulk Semiconductors: Implications for Enhancement of Solar Energy Conversion. *Nano Lett.* **2010**, *10*, 3019−3027.

(25) Ellingson, R. J.; Beard, M. C.; Johnson, J. C.; Yu, P.; Micic, O. I.; Nozik, A. J.; Shabaev, A.; Efros, A. L. Highly Efficient Multiple Exciton Generation in Colloidal PbSe and PbS Quantum Dots. *Nano Lett.* **2005**, *5*, 865−871.

(26) Beard, M. C.; Knutsen, K. P.; Yu, P.; Luther, J. M.; Song, Q.; Metzger, W. K.; Ellingson, R. J.; Nozik, A. J. Multiple Exciton Generation in Colloidal Silicon Nanocrystals. *Nano Lett.* **2007**, *7*, 2506−2512.

(27) Bonadeo, N. H.; Erland, J.; Gammon, D.; Park, D.; Katzer, D. S.; Steel, D. G. Coherent Optical Control of the Quantum State of a Single Quantum Dot. *Science* **1998**, *282*, 1473−1476.

(28) Xu, X.; Sun, B.; Berman, P. R.; Steel, D. G.; Bracker, A. S.; Gammon, D.; Sham, L. J. Coherent Optical Spectroscopy of a Strongly Driven Quantum Dot. *Science* **2007**, *317*, 929−932.

(29) Ouyang, M.; Awschalom, D. D. Coherent Spin Transfer between Molecularly Bridged Quantum Dots. *Science* **2003**, *301*, 1074−1078.

(30) Brown, K.; Lidar, D.; Whaley, K. Quantum Computing with Quantum Dots on Quantum Linear Supports. *Phys. Rev. A: At., Mol. Opt. Phys.* **2001**, *65*, 012307.

(31) Gupta, J. A.; Awschalom, D. D.; Peng, X.; Alivisatos, A. P. Spin Coherence in Semiconductor Quantum Dots. *Phys. Rev. B* **1999**, *59*, R10421−R10424.

(32) Chen, O.; Chen, X.; Yang, Y.; Lynch, J.; Wu, H.; Zhuang, J.; Cao, Y. C. Synthesis of Metal−Selenide Nanocrystals Using Selenium Dioxide as the Selenium Precursor. *Angew. Chem., Int. Ed.* **2008**, *47*, 8638−8641.

(33) von Grünberg, H. H. Energy Levels of CdSe Quantum Dots: Wurtzite versus Zinc-Blende Structure. *Phys. Rev. B* **2013**, *55*, 2293−2302.

(34) Karel Čapek, R.; Moreels, I.; Lambert, K.; De Muynck, D.; Zhao, Q.; Van Tomme, A.; Vanhaecke, F.; Hens, Z. Optical Properties of Zincblende Cadmium Selenide Quantum Dots. *J. Phys. Chem. C* **2010**, *114*, 6371−6376.

(35) Norris, D. J.; Bawendi, M. G. Measurement and Assignment of the Size-Dependent Optical Spectrum in CdSe Quantum Dots. *Phys. Rev. B* **1996**, *53*, 16338−16346.
(36) Norris, D. J.; Sacra, A.; Murray, C. B.; Bawendi, M. G. Measurement of the Size Dependent Hole Spectrum in CdSe Quantum Dots. *Phys. Rev. Lett.* **1994**, *72*, 2612−2615.
(37) Klimov, V. I.; McBranch, D. W.; Leatherdale, C. A.; Bawendi, M. G. Electron and Hole Relaxation Pathways in Semiconductor Quantum Dots. *Phys. Rev. B* **1999**, *60*, 13740−13749.
(38) Klimov, V.; Bolivar, P. H.; Kurz, H. Ultrafast Carrier Dynamics in Semiconductor Quantum Dots. *Phys. Rev. B* **1996**, *53*, 1463−1467.
(39) Efros, A. L.; Kharchenko, V. A.; Rosen, M. Breaking the Phonon Bottleneck in Nanometer Quantum Dots: Role of Auger-Like Processes. *Solid State Commun.* **1995**, *93*, 281−284.
(40) Kilina, S. V.; Kilin, D. S.; Prezhdo, O. V. Breaking the Phonon Bottleneck in PbSe and CdSe Quantum Dots: Time-Domain Density Functional Theory of Charge Carrier Relaxation. *ACS Nano* **2009**, *3*, 93−99.
(41) Brus, L. E. A Simple Model for the Ionization Potential, Electron Affinity, and Aqueous Redox Potentials of Small Semiconductor Crystallites. *J. Chem. Phys.* **1983**, *79*, 5566−5571.
(42) Alivisatos, A. P.; Harris, A. L.; Levinos, N. J.; Steigerwald, M. L.; Brus, L. E. Electronic States of Semiconductor Clusters: Homogeneous and Inhomogeneous Broadening of the Optical Spectrum. *J. Chem. Phys.* **1988**, *89*, 4001−4011.
(43) Scholes, G. D. Controlling the Optical Properties of Inorganic Nanoparticles. *Adv. Funct. Mater.* **2008**, *18*, 1157−1172.
(44) Salvador, M. R.; Hines, M. A.; Scholes, G. D. Exciton−Bath Coupling and Inhomogeneous Broadening in the Optical Spectroscopy of Semiconductor Quantum Dots. *J. Chem. Phys.* **2003**, *118*, 9380−9388.
(45) Cui, J.; Beyler, A. P.; Marshall, L. F.; Chen, O.; Harris, D. K.; Wanger, D. D.; Brokmann, X.; Bawendi, M. G. Direct Probe of Spectral Inhomogeneity Reveals Synthetic Tunability of Single-Nanocrystal Spectral Linewidths. *Nat. Chem.* **2013**, *5*, 602−606.
(46) Klimov, V. I.; McBranch, D. W. Femtosecond 1p-to-1s Electron Relaxation in Strongly Confined Semiconductor Nanocrystals. *Phys. Rev. Lett.* **1998**, *80*, 4028−4031.
(47) Nirmal, M.; Norris, D. J.; Kuno, M.; Bawendi, M. G.; Efros, A. L.; Rosen, M. Observation of the "Dark Exciton" in CdSe Quantum Dots. *Phys. Rev. Lett.* **1995**, *75*, 3728−3731.
(48) Klimov, V. I. Optical Nonlinearities and Ultrafast Carrier Dynamics in Semiconductor Nanocrystals. *J. Phys. Chem. B* **2000**, *104*, 6112−6123.
(49) Wong, C. Y.; Scholes, G. D. Using Two-Dimensional Photon Echo Spectroscopy to Probe the Fine Structure of the Ground State Biexciton of CdSe Nanocrystals. *J. Lumin.* **2011**, *131*, 366−374.
(50) Moody, G.; Singh, R.; Li, H.; Akimov, I. A.; Bayer, M.; Reuter, D.; Wieck, A. D.; Bracker, A. S.; Gammon, D.; Cundiff, S. T. Influence of Confinement on Biexciton Binding in Semiconductor Quantum Dot Ensembles Measured with Two-Dimensional Spectroscopy. *Phys. Rev. B* **2013**, *87*, 041304.
(51) Seibt, J.; Hansen, T.; Pullerits, T. 3D Spectroscopy of Vibrational Coherences in Quantum Dots: Theory. *J. Phys. Chem. B* **2013**, *117*, 11124−11133.
(52) Seibt, J.; Pullerits, T. Beating Signals in 2D Spectroscopy: Electronic or Nuclear Coherences? Application to a Quantum Dot Model System. *J. Phys. Chem. C* **2013**, *117*, 18728−18737.
(53) Zheng, H.; Caram, J. R.; Dahlberg, P. D.; Rolczynski, B. S.; Viswanathan, S.; Dolzhnikov, D. S.; Khadivi, A.; Talapin, D. V.; Engel, G. S. Dispersion-Free Continuum Two-Dimensional Electronic Spectrometer. Submitted.
(54) Lozovoy, V. V.; Pastirk, I.; Dantus, M. Multiphoton Intrapulse Interference. Ultrashort Laserpulse Spectral Phase Characterization and Compensation. *Opt. Lett.* **2004**, *29*, 775−777.
(55) Trebino, R. *Frequency-Resolved Optical Gating: The Measurement of Ultrashort Laser Pulses*; Kluwer Academic Publishers: Boston, MA, 2002.
(56) Hybl, J.; Albrecht, A.; Faeder, S.; Jonas, D. Two-Dimensional Electronic Spectroscopy. *Chem. Phys. Lett.* **1998**, *297*, 307−313.
(57) Jonas, D. M. Two-Dimensional Femtosecond Spectroscopy. *Annu. Rev. Phys. Chem.* **2003**, *54*, 425−463.
(58) Brixner, T.; Mančal, T.; Stiopkin, I. V.; Fleming, G. R. Phase-Stabilized Two-Dimensional Electronic Spectroscopy. *J. Chem. Phys.* **2004**, *121*, 4221.
(59) Cho, M. Coherent Two-Dimensional Optical Spectroscopy. *Chem. Rev.* **2008**, *108*, 1331−1418.
(60) Myers, J. A.; Lewis, K. L. M.; Fuller, F. D.; Tekavec, P. F.; Yocum, C. F.; Ogilvie, J. P. Two-Dimensional Electronic Spectroscopy of the D1-D2-cyt B559 Photosystem II Reaction Center Complex. *J. Phys. Chem. Lett.* **2010**, *1*, 2774−2780.
(61) Cowan, M. L.; Ogilvie, J. P.; Miller, R. J. D. Two-Dimensional Spectroscopy Using Diffractive Optics Based Phased-Locked Photon Echoes. *Chem. Phys. Lett.* **2004**, *386*, 184−189.
(62) Hybl, J. D.; Ferro, A. A.; Jonas, D. M. Two-Dimensional Fourier Transform Electronic Spectroscopy. *J. Chem. Phys.* **2001**, *115*, 6606−6622.
(63) Singh, V. P.; Fidler, A. F.; Rolczynski, B. S.; Engel, G. S. Independent Phasing of Rephasing and Non-Rephasing 2D Electronic Spectra. *J. Chem. Phys.* **2013**, *139*, 084201−084205.
(64) Cheng, Y.-C.; Fleming, G. R. Coherence Quantum Beats in Two-Dimensional Electronic Spectroscopy. *J. Phys. Chem. A* **2008**, *112*, 4254−4260.
(65) Cheng, Y.; Engel, G.; Fleming, G. Elucidation of Population and Coherence Dynamics Using Cross-Peaks in Two-Dimensional Electronic Spectroscopy. *Chem. Phys.* **2007**, *341*, 285−295.
(66) Calhoun, T. R.; Ginsberg, N. S.; Schlau-Cohen, G. S.; Cheng, Y.-C.; Ballottari, M.; Bassi, R.; Fleming, G. R. Quantum Coherence Enabled Determination of the Energy Landscape in Light-Harvesting Complex II. *J. Phys. Chem. B* **2009**, *113*, 16291−16295.
(67) Egorova, D. Detection of Electronic and Vibrational Coherences in Molecular Systems by 2D Electronic Photon Echo Spectroscopy. *Chem. Phys.* **2008**, *347*, 166−176.
(68) Nemeth, A.; Milota, F.; Mancal, T.; Lukes, V.; Hauer, J.; Kauffmann, H. F.; Sperling, J. Vibrational Wave Packet Induced Oscillations in Two-Dimensional Electronic Spectra. I. Experiments. *J. Chem. Phys.* **2010**, *132*, 184514.
(69) Mancal, T.; Nemeth, A.; Milota, F.; Lukes, V.; Kauffmann, H. F.; Sperling, J. Vibrational Wave Packet Induced Oscillations in Two-Dimensional Electronic Spectra. II. Theory. *J. Chem. Phys.* **2010**, *132*, 184515.
(70) Christensson, N.; Milota, F.; Hauer, J.; Sperling, J.; Bixner, O.; Nemeth, A.; Kauffmann, H. F. High Frequency Vibrational Modulations in Two-Dimensional Electronic Spectra and Their Resemblance to Electronic Coherence Signatures. *J. Phys. Chem. B* **2011**, *115*, 5383−5391.
(71) Caram, J. R.; Fidler, A. F.; Engel, G. S. Excited and Ground State Vibrational Dynamics Revealed by Two-Dimensional Electronic Spectroscopy. *J. Chem. Phys.* **2012**, *137*, 024507−024510.
(72) Turner, D. B.; Wilk, K. E.; Curmi, P. M. G.; Scholes, G. D. Comparison of Electronic and Vibrational Coherence Measured by Two-Dimensional Electronic Spectroscopy. *J. Phys. Chem. Lett.* **2011**, *2*, 1904−1911.
(73) Kambhampati, P. Unraveling the Structure and Dynamics of Excitons in Semiconductor Quantum Dots. *Acc. Chem. Res.* **2010**, *44*, 1−13.
(74) Sewall, S. L.; Cooney, R. R.; Anderson, K. E. H.; Dias, E. A.; Sagar, D. M.; Kambhampati, P. State-Resolved Studies of Biexcitons and Surface Trapping Dynamics in Semiconductor Quantum Dots. *J. Chem. Phys.* **2008**, *129*, 084701.
(75) Saari, J. I.; Dias, E. A.; Reifsnyder, D.; Krause, M. M.; Walsh, B. R.; Murray, C. B.; Kambhampati, P. Ultrafast Electron Trapping at the Surface of Semiconductor Nanocrystals: Excitonic and Biexcitonic Processes. *J. Phys. Chem. B* **2012**, *117*, 4412−4421.
(76) Caram, J. R.; Zheng, H.; Dahlberg, P. D.; Rolczynski, B. S.; Griffin, G. B.; Dolzhnikov, D. S.; Talapin, D. V.; Engel, G. S. Exploring Size and State Dynamics in Polydisperse CdSe Quantum Dots

Explored Using Two-Dimensional Electronic Spectroscopy. Submitted.
(77) Mukamel, S. *Nonlinear Optical Spectroscopy*; Oxford: New York, 1995.
(78) Thomas, D.; Michael, F. Coherent Phonons in Bulk and Low-Dimensional Semiconductors. *Coherent Vibrational Dynamics*; CRC Press: Boca, Raton, FL, 2007; pp 129−172.
(79) Fransted, K. A.; Caram, J. R.; Hayes, D.; Engel, G. S. Two-Dimensional Electronic Spectroscopy of Bacteriochlorophyll a in Solution: Elucidating the Coherence Dynamics of the Fenna−Matthews−Olson Complex Using Its Chromophore as a Control. *J. Chem. Phys.* **2012**, *137*, 125101−125109.
(80) Hershberger, M. A.; Moran, A. M.; Scherer, N. F. New Insights into Response Functions of Liquids by Electric Field-Resolved Polarization Emission Time Measurements. *J. Phys. Chem. B* **2011**, *115*, 5617−5624.
(81) Wilmshurst, J. K.; Bernstein, H. J. The Infrared and Raman Spectra of Toluene, Toluene-A-D3, M-Xylene, and M-Xylene-Aα'-D6. *Can. J. Chem.* **1957**, *35*, 911−925.
(82) Collini, E.; Wong, C. Y.; Wilk, K. E.; Curmi, P. M. G.; Brumer, P.; Scholes, G. D. Coherently Wired Light-Harvesting in Photosynthetic Marine Algae at Ambient Temperature. *Nature* **2010**, *463*, 644−647.
(83) Panitchayangkoon, G.; Hayes, D.; Fransted, K. A.; Caram, J. R.; Harel, E.; Wen, J.; Blankenship, R. E.; Engel, G. S. Long-Lived Quantum Coherence in Photosynthetic Complexes at Physiological Temperature. *Proc. Natl. Acad. Sci. U.S.A.* **2010**, *107*, 12766−12770.
(84) Kreisbeck, C.; Kramer, T.; Aspuru-Guzik, A. Disentangling Electronic and Vibronic Coherences in Two-Dimensional Echo Spectra. *J. Phys. Chem. B* **2013**, *117*, 9380−9385.
(85) Lee, H.; Cheng, Y.-C.; Fleming, G. R. Coherence Dynamics in Photosynthesis: Protein Protection of Excitonic Coherence. *Science* **2007**, *316*, 1462−1465.
(86) Hayes, D.; Panitchayangkoon, G.; Fransted, K. A.; Caram, J. R.; Wen, J.; Freed, K. F.; Engel, G. S. Dynamics of Electronic Dephasing in the Fenna−Matthews−Olson Complex. *New J. Phys.* **2010**, *12*, 065042.
(87) Caram, J. R.; Engel, G. S. Extracting Dynamics of Excitonic Coherences in Congested Spectra of Photosynthetic Light Harvesting Antenna Complexes. *Faraday Discuss.* **2011**, *153*, 93−104.
(88) Caram, J. R.; Lewis, N. H. C.; Fidler, A. F.; Fidler, A. F.; Engel, G. S. Signatures of Correlated Excitonic Dynamics in Two-Dimensional Spectroscopy of the Fenna−Matthew−Olson Photosynthetic Complex. *J. Chem. Phys.* **2012**, *136*, 104505.
(89) Fidler, A. F.; Caram, J. R.; Hayes, D.; Engel, G. S. Towards a Coherent Picture of Excitonic Coherence in the Fenna−Matthews−Olson Complex. *J. Phys. B: At., Mol. Opt. Phys.* **2012**, *45*, 154013.
(90) Mukamel, S. Comment on "Coherence and Uncertainty in Nanostructured Organic Photovoltaics". *J. Phys. Chem. A* **2013**, *117*, 10563−10564.
(91) Panitchayangkoon, G.; Hayes, D.; Fransted, K. A.; Caram, J. R.; Harel, E.; Wen, J.; Blankenship, R. E.; Engel, G. S. Long-Lived Quantum Coherence in Photosynthetic Complexes at Physiological Temperature. *Proc. Natl. Acad. Sci. U.S.A.* **2010**, *107*, 12766−12770.
(92) Collini, E.; Scholes, G. D. Coherent Intrachain Energy Migration in a Conjugated Polymer at Room Temperature. *Science* **2009**, *323*, 369−373.
(93) Collini, E.; Wong, C. Y.; Wilk, K. E.; Curmi, P. M. G.; Brumer, P.; Scholes, G. D. Coherently Wired Light-Harvesting in Photosynthetic Marine Algae at Ambient Temperature. *Nature* **2010**, *463*, 644−647.
(94) Hayes, D.; Griffin, G. B.; Engel, G. S. Engineering Coherence among Excited States in Synthetic Heterodimer Systems. *Science* **2013**, 1431−1434.
(95) Fidler, A. F.; Singh, V. P.; Long, P. D.; Dahlberg, P. D.; Engel, G. S. Time Scales of Coherent Dynamics in the Light-Harvesting Complex 2 (LH2) of *Rhodobacter sphaeroides*. *J. Phys. Chem. Lett.* **2013**, *4*, 1404−1409.
(96) Kubo, R. A Stochastic Theory of Line Shape. In *Advances in Chemical Physics*, John Wiley & Sons, Inc.: New York, 1969; pp 101−127.
(97) Tanimura, Y.; Kubo, R. Time Evolution of a Quantum System in Contact with a Nearly Gaussian−Markoffian Noise Bath. *J. Phys. Soc. Jpn.* **1989**, *58*, 101.
(98) Fisher, B. R.; Eisler, H.-J.; Stott, N. E.; Bawendi, M. G. Emission Intensity Dependence and Single-Exponential Behavior in Single Colloidal Quantum Dot Fluorescence Lifetimes. *J. Phys. Chem. B* **2003**, *108*, 143−148.
(99) Cho, M.; Vaswani, H. M.; Brixner, T.; Stenger, J.; Fleming, G. R. Exciton Analysis in 2D Electronic Spectroscopy. *J. Phys. Chem. B* **2005**, *109*, 10542−10556.
(100) McKimmie, L. J.; Lincoln, C. N.; Jasieniak, J.; Smith, T. A. Three-Pulse Photon Echo Peak Shift Measurements of Capped CdSe Quantum Dots. *J. Phys. Chem. C* **2009**, *114*, 82−88.
(101) Shim, S.; Rebentrost, P.; Valleau, S.; Aspuru-Guzik, A. Atomistic Study of the Long-Lived Quantum Coherences in the Fenna−Matthews−Olson Complex. *Biophys. J.* **2012**, *102*, 649−660.
(102) Tiwari, V.; Peters, W. K.; Jonas, D. M. Electronic Resonance with Anticorrelated Pigment Vibrations Drives Photosynthetic Energy Transfer Outside the Adiabatic Framework. *Proc. Natl. Acad. Sci. U.S.A.* **2012**, *110*, 1203−1208.
(103) Christensson, N.; Kauffmann, H. F.; Pullerits, T.; Mancal, T. Origin of Long-Lived Coherences in Light-Harvesting Complexes. *J. Phys. Chem. B* **2012**, *116*, 7449−7454.
(104) Chin, A. W.; Prior, J.; Rosenbach, R.; Caycedo-Soler, F.; Huelga, S. F.; Plenio, M. B. The Role of Non-Equilibrium Vibrational Structures in Electronic Coherence and Recoherence in Pigment−Protein Complexes. *Nat. Phys.* **2013**, *9*, 113−118.
(105) Pandey, A.; Guyot-Sionnest, P. Slow Electron Cooling in Colloidal Quantum Dots. *Science* **2008**, *322*, 929−932.
(106) Pelzer, K. M.; Griffin, G. B.; Gray, S. K.; Engel, G. S. Inhomogeneous Dephasing Masks Coherence Lifetimes in Ensemble Measurements. *J. Chem. Phys.* **2012**, *136*, 164508−164506.